

Dimuon production by laser-wakefield accelerated electrons

A.I. Titov^{a,b,c}, B. Kämpfer^{a,d} and H. Takabe^c

^a*Forschungszentrum Dresden-Rossendorf, 01314 Dresden, Germany*

^b*Bogoliubov Laboratory of Theoretical Physics, JINR, Dubna 141980, Russia*

^c*Institute of Laser Engineering, Yamada-oka, Suita, Osaka 565-0871, Japan*

^d*Institut für Theoretische Physik, TU Dresden, 01062 Dresden, Germany*

Abstract

We analyze $\mu^+\mu^-$ pair production generated by high-energy electrons emerging from a laser-wakefield accelerator. The $\mu^+\mu^-$ pairs are created in a solid thick high- Z target, following the electron accelerating plasma region. Numerical estimates are presented for electron beams obtained presently in the LBL TW laser experiment [1] and possible future developments. Reactions induced by the secondary bremsstrahlung photons dominate the dimuon production. According to our estimates, a 20 pC electron bunch with energy of 1 (10) GeV may create about 200 (6000) muon pairs. The produced μ^\pm can be used in studying various aspects of muon-related physics in table top installations. This may be considered as an important step towards the investigation of more complicated elementary processes induced by laser driven electrons.

PACS numbers: 12.20.Ds,13.60.Le,41.75.Jv

I. INTRODUCTION

The possibility to produce strong electric fields of the order of 10 – 100 GV/m with present laser facilities is a great advantage for laser-wakefield accelerators [2] which allows, in principle, to construct compact accelerating devices for particle and nuclear physics. The successful production of high-quality electron beams in such laser-driven accelerators with electron energies of the order of 1 GeV has been reported recently [1, 3, 4]. Electron beams with energies exceeding 1 GeV are interesting for many applications in particle physics, such as investigating the properties and production mechanisms of vector and exotic scalar mesons in photo/electroproduction [5, 6], excitation of baryon resonances with the aim of studying their properties and search for missing resonances [7], strangeness photoproduction [8] etc. Another subject is related to the neutrino physics. For example, neutrino oscillations need two types of neutrinos, at least. They may be obtained in muon decays $\mu^+ \rightarrow e^+ + \nu_e + \bar{\nu}_\mu$ and $\mu^- \rightarrow e^- + \bar{\nu}_e + \nu_\mu$, where muons and electrons neutrinos (or antineutrinos) are produced in equal parts. Therefore, it is interesting to estimate whether the high-energy laser-driven electrons can produce a sizeable amount of muon pairs for future applications.

Recall that the present generation of the high-energy neutrino beams are made by decays of charged pions and kaons in flight in a long decay channel. In this case, the neutrino (antineutrino) beams mostly consists of ν_μ ($\bar{\nu}_\mu$) with rather small admixture of electron neutrinos. The idea to use a storage ring of muons as a source of high-energy and high-intensity neutrino beam has been discussed in Refs. [9, 10]. It is assumed that the muons are produced in two-body decays $\pi^+ \rightarrow \mu^+ + \nu_\mu$ and $K^+ \rightarrow \mu^+ + \nu_\mu$ and then stored in a ring with subsequent decay into an electron and two neutrinos. The pions (kaons) in turn, are produced in proton-proton and (or) in proton-nucleus collisions with high-intensity proton beams [11]. Together with neutrino oscillation, such high-intensity muon sources may be used in studying other fundamental problems of lepton physics, say the search for lepton flavor violation [12] and the measurement of the muon's anomalous magnetic moment [13]. The idea to use a laser-driven proton beam for investigating different aspects of the neutrino oscillations was discussed for the first time in Ref. [14].

The aim of present paper is to analyze the possibility of muon pair creation in the interaction of high-energy laser driven electrons within a heavy (high- Z) target in a table top configuration. The electromagnetic sources of the $\mu^+\mu^-$ (dimuon) production are described

by the following elementary processes

$$\gamma + A \rightarrow A + \mu^+ \mu^-, \quad (1)$$

$$e + A \rightarrow e' + A + \mu^+ \mu^-. \quad (2)$$

In the first case (1) the dimuons are produced in the interaction of real (bremsstrahlung) photons within the electric field of the high- Z target nuclei. This is an analog of well known Bethe-Heitler process of the electron-positron production. In the second case (2), the dimuons are produced in the interaction of high-energy electrons with nuclei (so called trident process). These two reactions are depicted in Fig. 1. In some sense these reactions

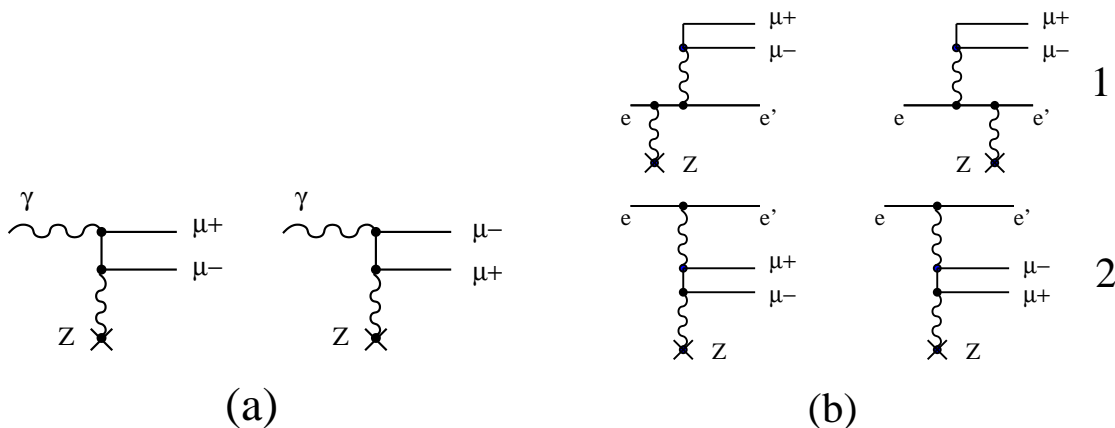


FIG. 1: Diagrammatic representation of dimuon production processes in electromagnetic interactions. (a) Bethe-Heitler process $\gamma + A \rightarrow A + \mu^+ \mu^-$. (b) Electron induced reaction $e + A \rightarrow e + A + \mu^+ \mu^-$.

are similar to the dielectron production by laser-driven relativistic electrons at few dozen MeV analyzed by Nakashima and Takabe [15] and other authors (see, for example, Ref. [16]). Therefore, our investigation may be considered as a continuation of these studies, but with the focus on dimuon production. For other avenues towards laser-generated muon pair production cf. Refs. [17, 18]. Dimuon production in electron-positron-photon plasmas was estimated in [19].

Our paper is organized as follows. In Sect. II, we recall the relevant elementary electromagnetic processes. Estimates of the dimuon yield are presented in Sect. III, where the energy loss and attenuation of the primary electron beam and the secondary photon bremsstrahlung spectrum are accounted for. Hadronic processes are briefly discussed in Sect. IV. Our conclusions can be found in Sect. V.

II. ELEMENTARY CROSS SECTIONS

The differential cross section of the dimuon production in the reaction Eq. (1) reads

$$d\sigma^{\gamma A} = \frac{Z^2 \alpha^3}{4\pi} \frac{|\mathbf{q}|}{|\mathbf{k}|} |T^{\gamma A}|^2 \sqrt{M_{\mu^+\mu^-}^2 - 4\mu^2} dM_{\mu^+\mu^-} d\cos\theta_q d\Omega_{\mu^+}, \quad (3)$$

where \mathbf{k} and \mathbf{q} are the spatial parts of the incoming photon momentum and the total momentum of the outgoing muon pair $q = p_{\mu^+} + p_{\mu^-}$ with the invariant mass of the muon pair $M_{\mu^+\mu^-}^2 = q^2$; μ denotes the muon mass, θ_q is the polar angle of the direction of flight of dimuon, Ω_{μ^+} is the solid angle of the direction of the velocity of the μ^+ meson in the rest frame of the dimuon; Z and α stand for the nuclear charge and the fine structure constant ($\alpha = 1/137$), respectively; $T^{\gamma A}$ is the invariant amplitude and averaging over photon polarization and summation over μ^\pm spin states is provided in $|T^{\gamma A}|^2$. The quantization axis z is chosen along velocity of incoming photon, and the production plane is defined by the vectors \mathbf{k} and \mathbf{q} . The differential cross section depends on the initial energy and four kinematical variables, which define the final state.

In case of the $e + A \rightarrow e' + A + \mu^+ \mu^-$ reaction Eq. (2) we have relevant two sub-processes. One corresponds to the electron scattering off the nucleus. In the second case, one of the outgoing muons interacts with the atomic nucleus. These two cases are marked in Fig. 1 (b) as "1" and "2", respectively. The total amplitude is the coherent sum of all four amplitudes. The differential cross section for this reaction depends on seven kinematical variables, which define the final state of the outgoing leptons and recoil nucleus, and it has the form

$$d\sigma^{eA} = \frac{Z^2 \alpha^4}{16\pi^3} \frac{|\mathbf{p}_{e'}|}{|\mathbf{p}_e|} |T^{eA}|^2 \sqrt{M_{\mu^+\mu^-}^2 - 4\mu^2} |\mathbf{q}| dE_q dM_{\mu^+\mu^-} d\cos\theta_{e'} d\Omega_q d\Omega_{\mu^+}, \quad (4)$$

where \mathbf{p}_e and $\mathbf{p}_{e'}$ are three momenta of the incoming and outgoing electrons, respectively, $\theta_{e'}$ is the polar angle of the direction of flight of the outgoing electron, $E_q = \sqrt{\mathbf{q}^2 + M_{\mu^+\mu^-}^2}$ is the energy of the muon pair; T^{eA} is the invariant amplitude and averaging over initial electron spin projections and summation over the final fermion spin states is understood in $|T^{eA}|^2$; the quantization axis (\mathbf{z}) is along velocity of the incoming electron, and $\mathbf{y} = [\mathbf{p}_e \times \mathbf{p}_{e'}]/|\mathbf{p}_e||\mathbf{p}_{e'}|$.

The invariant amplitudes for reactions in Eqs. (1) and (2) are calculated in the lowest order of perturbation theory analog to the electron-positron production in γA and eA interactions [20]. The amplitude for the γA reaction reads

$$T^{\gamma A} = -\frac{1}{\kappa_\gamma^2} \bar{u}_{\mu^-} \left[\gamma_0 \frac{\not{g}_1 + \mu}{g_1^2 - \mu^2} \gamma_\alpha - \gamma_\alpha \frac{\not{g}_2 - \mu}{g_2^2 - \mu^2} \gamma_0 \right] v_{\mu^+} \varepsilon_\gamma^\alpha, \quad (5)$$

where u and v are the Dirac spinors of the outgoing μ^- and μ^+ muons, respectively, ε_γ is the polarization vector of incoming photons, $g_1 = k - p_{\mu^+}$, $g_2 = k - p_{\mu^-}$, and $\kappa_\gamma = k - q$. The notation \not{p} means the four product $\gamma_\alpha p^\alpha$, where γ_α ($\alpha = 0, 1, 2, 3$) are Dirac's γ matrices.

Correspondingly, for the eA reaction we have

$$T^{eA} = T_1^{eA} + T_2^{eA}$$

with

$$T_1^{eA} = -\frac{1}{\kappa_e^2 q^2} \left(\bar{u}_{e'} \left[\gamma_0 \frac{\not{p}_1 + m_e}{p_1^2 - m_e^2} \gamma_\alpha - \gamma_\alpha \frac{\not{p}_2 + m_e}{p_2^2 - m_e^2} \gamma_0 \right] u_e \right) (\bar{u}_{\mu^-} \gamma^\alpha v_{\mu^+}) , \quad (6)$$

$$T_2^{eA} = -\frac{1}{\kappa_e^2 q'^2} (\bar{u}_{e'} \gamma^\alpha u_e) \left(\bar{u}_{\mu^-} \left[\gamma_0 \frac{\not{p}_3 + \mu}{p_3^2 - \mu^2} \gamma_\alpha - \gamma_\alpha \frac{\not{p}_4 - \mu}{p_4^2 - \mu^2} \gamma_0 \right] v_{\mu^+} \right) , \quad (7)$$

where $q' = p_e - p_{e'}$, $p_1 = p_e - q$, $p_2 = p_{e'} + q$, $p_3 = q' - p_{\mu^+}$, $p_4 = q' - p_{\mu^-}$, and $\kappa_e = q' - q$.

The effects of nuclear size and higher-order Coulomb corrections are small [21]; the effects of the atomic electron screening [22, 23] are neglected here as the production processes happen in the high-field region near the target nuclei. The corresponding cross sections Eqs. (3) and (4) are evaluated numerically without any additional approximation.

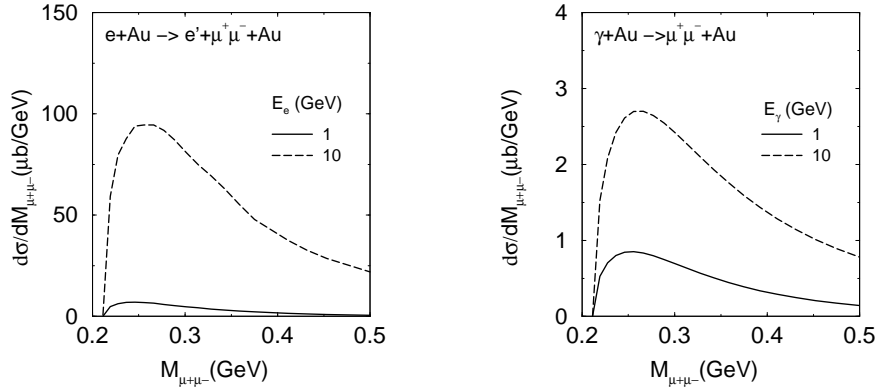


FIG. 2: Differential cross sections of dimuon production in eA (left panel) and γA (right panel) interactions as a function of the invariant dimuon mass $M_{\mu^+\mu^-}$. The solid and dashed curves correspond to initial energies of 1 and 10 GeV, respectively.

The invariant-mass distributions for γA and eA reactions are shown in Fig. 2. In this case, the corresponding cross sections are calculated as a function of the invariant mass $M_{\mu^+\mu^-}$ integrating over the other variables in Eqs. (3) and (4). All calculations are done for a gold target. The initial electron energies are chosen to be 1 and 10 GeV. For 1 GeV we follow the laser accelerator conditions of Ref. [1]. The case of 10 GeV may be considered as

prediction for future high-energy table top electron accelerators being under consideration now [24, 25, 26]. For simplicity, in case of the γA reaction, the elementary cross sections are calculated at $E_\gamma = 1$ and 10 GeV. Below, for the estimate of the dimuon yield, we fold the elementary cross section with the bremsstrahlung photon distribution for all kinematically allowed photon energies.

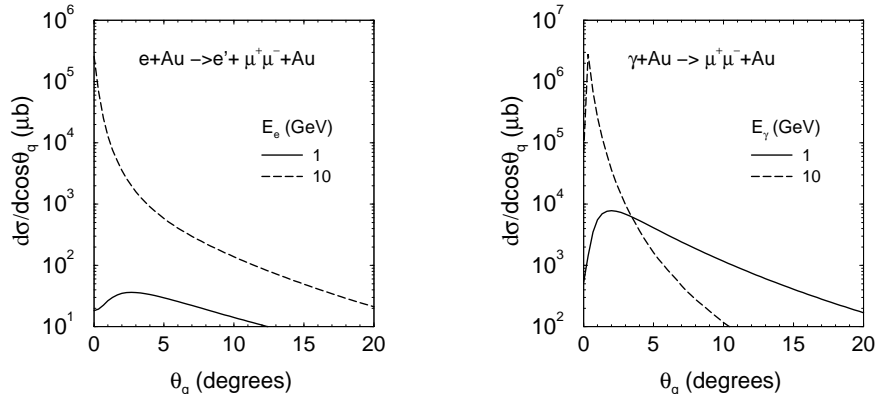


FIG. 3: Differential cross sections of dimuon production in $e A$ (left panel) and γA (right panel) reactions as a function of polar angle θ_q . The solid and dashed curves correspond to initial energies 1 and 10 GeV, respectively.

Fig. 2 demonstrates that the cross section of the electron induced reaction is smaller by two order of magnitude than the corresponding cross section in the photon induced reaction. This is mainly because of an additional vertex with additional factor α . Both distributions exhibit a maximum slightly above $\sim 2\mu$. This means that the relative kinetic energy of the two muons in a pair is small, i.e. they flight close to each other.

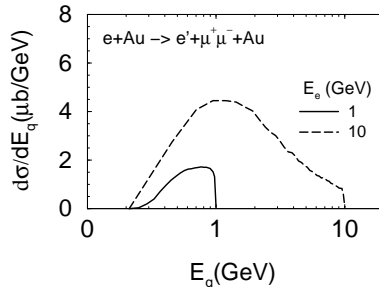


FIG. 4: The differential cross section for electron induced muon pair production reaction as a function of dimuon energy E_q . The solid and dashed curves correspond to initial energies 1 and 10 GeV, respectively.

The differential cross sections as a function of the polar angle of the direction of flight of the muon pair θ_q integrated over the other variables are shown in Fig. 3. One can see that the cross sections are peaked at the forward direction, especially for $E_{e,\gamma} = 10$ GeV. The knowledge of the spatial structure of the outgoing muon flux is important for the design of the devices for muon sources.

The differential cross section of the reaction $e + A \rightarrow e' + \mu^+ \mu^- + A$ as a function of the dimuon energy E_q is presented in Fig. 4. One can see a wide spread of this distribution with a maximum around 1 GeV for initial electron energy of 10 GeV, while for 1 GeV electrons the dimuon energy displays a plateau above 0.6 GeV till the kinematical limit. Since the kinetic energy of the relative motion of μ^+ and μ^- within a pair is small ($E_{\mu^\pm} \simeq E_q/2$), the energy distribution of the individual muons may be approximated as $d\sigma/dE_{\mu^+} \simeq d\sigma/dE_{\mu^-} \simeq d\sigma/dE_q|_{E_{\mu^\pm}=E_q/2}$.

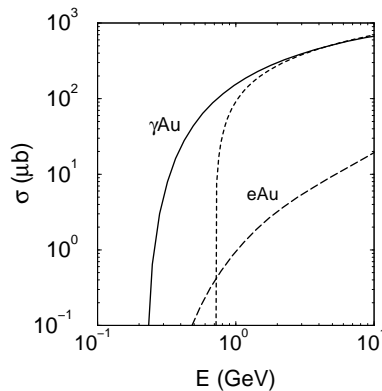


FIG. 5: The total cross section of the dimuon production in γA (solid curve) and $e A$ (dashed curve) reactions as a function of initial energy. The dotted curve corresponds to the high-energy approximation Eq. (8).

The total cross sections of the dimuon production as a function of the initial energy are shown in Fig. 5. One can see a steep increase of the cross sections with energy. We note that in the ultra-relativistic case with $E_\gamma \gg \mu$ the total cross section of the reaction $\gamma A \rightarrow \mu^+ \mu^- A$ may be described by [20]

$$\sigma \simeq \frac{28}{9} Z_A^2 \alpha r_0^{\mu 2} \left(\ln \frac{2E_\gamma}{\mu} - \frac{109}{42} \right), \quad (8)$$

where $r_0^\mu = \alpha/\mu$ is the classical muon radius. The corresponding cross section is shown in Fig. 5 by the dotted curve showing that the ultra-relativistic behavior sets in at $E_\gamma \gtrsim 3$ GeV.

The total cross sections for γA and $e A$ reactions reach $300 \mu\text{b}$ and $3 \mu\text{b}$, respectively, at $E_{\gamma(e)} \simeq 2 \text{ GeV}$. Similarly to the differential cross sections, the difference between the two reactions is about two orders of magnitude, mainly due to an additional power of α in the $e A$ cross section.

III. DIMUON YIELDS

Using the above elementary cross sections one can estimate the dimuon yield for given electron beam and target properties. For the former ones we use the conditions of electron beams as reported for the laser-wakefield accelerator in Ref. [1]. The electron energy is about $0.5 - 1 \text{ GeV}$ and the electron flux is about 20 pC which corresponds to $N_0^e \simeq 1.248 \times 10^8$ electrons in a bunch. In our estimates we assume the same flux for electron energies up to 10 GeV . We consider a gold target with thickness of $L = 0.1 - 1 \text{ cm}$.

Strictly speaking, the particle production in interactions of the high-energy electrons with heavy target nuclei must be evaluated by transport-kinetic models (see, for example, Refs. [15, 16]). However, for a first qualitative estimate of the dimuon yield one can use an analytical approach, similar to that developed in Ref. [27].

Consider first the dimuon yield which stems from elementary $eA \rightarrow e' + \mu^+ \mu^- + A$ reactions. It may be expressed as

$$dN^{\mu^+ \mu^-} = \frac{N_A \rho_A}{A} \int_0^L dl N^e(l) d\sigma^{eA \rightarrow e' \mu^+ \mu^- A}(E_e(l)), \quad (9)$$

where A is the atomic weight, N_A is Avogadro's number, ρ_A denotes the target density, $d\sigma^{eA \rightarrow e' \mu^+ \mu^- A}$ is the elementary cross section of the dimuon production discussed above. For the sake of simplicity, we neglect the energy spread in the bunch taking the electron energy at the central positions of the energy distribution. This seems to be reasonable, because the energy spreading reported in [1] is less than 100 MeV at $E_e \simeq 1 \text{ GeV}$.

Propagating through the target material the electron beam loses its intensity and energy. The energy loss is described by [20]

$$\frac{dE_e}{dl} = -E_e \frac{N_A \rho_A \alpha Z_A^2 r_0^2}{A} \left(4 \ln \frac{183}{Z_A^{1/3}} + \frac{2}{9} \right) \quad (10)$$

with $r_0^e = \alpha/m_e \simeq 2.18 \times 10^{-13} \text{ cm}$. For the gold target with $A = 197$ and $Z_A = 79$ this

leads to the formula

$$E_e(l) \simeq E_e^0 \exp(-l/l_0) \quad (11)$$

with $l_0 \simeq 0.513$ cm. The electron beam absorption in the target may be accounted for by a linear dependence

$$N^e(l) \simeq N_0^e(1 - l/L_{\max}(E_e^0)) , \quad (12)$$

where N_0^e is the initial beam intensity and L_{\max} stands for the maximum distance traveled by the high-energy electrons. For the gold target one can use $L_{\max} \simeq 1.44$ cm at $E_e = 0.5$ GeV which may be extrapolated as $L_{\max}(E) \simeq 0.23 E^{0.3}$ cm with E in GeV [28]. Both, the decrease of the beam intensity and the energy loss lead to a decrease of the effectiveness of the dimuon production in the target material. However, the effect of the energy loss is significantly greater than the effect of intensity depletion since the scale parameter l_0 in Eq. (11) is much smaller than L_{\max} .

The yield of dimuons, produced by secondary real photons created at the distance l behind the target front side, reads

$$dN^{\mu^+\mu^-} = \frac{N_A \rho_A}{A} \int_0^L dl \int dE_\gamma \frac{dN_\gamma(l)}{dE_\gamma} (L - l) d\sigma^{\gamma A \rightarrow \mu^+\mu^- A}(E_\gamma) , \quad (13)$$

where $d\sigma^{\gamma A \rightarrow \mu^+\mu^- A}$ is the above cross section of the dimuon production in the elementary γA interaction, and $dN_\gamma(l)/dE_\gamma$ denotes the distribution of bremsstrahlung photons with energy E_γ at distance l

$$\frac{dN_\gamma(l)}{dE_\gamma} = \frac{N_A \rho_A}{A} N^e(l) \frac{d\sigma_\gamma(E_e(l), E_\gamma)}{dE_\gamma} , \quad (14)$$

where $N^e(l)$ is defined by Eq. (12) and the current electron energy $E_e(l)$ from Eq. (11) is to be used. For the angular-integrated bremsstrahlung cross section $d\sigma_\gamma(E_e, E_\gamma)/dE_\gamma$ we adopt a parametrization motivated by the analytical expression of Ref. [20]

$$\frac{E_\gamma}{Z_A^2} \frac{d\sigma_\gamma}{dE_\gamma} = \frac{4\alpha r_0^2 F(E_e, E_\gamma)}{E_e^2} \left((E_e^2 + E_{e'}^2 - \frac{2}{3} E_e E_{e'}) \ln 183 Z_A^{-1/3} + \frac{E_e E_{e'}}{9} \right) , \quad (15)$$

where $E_{e'} = E_e - E_\gamma$ and $F(E_e, E_\gamma) = 0.91 \tanh(E_{e'}/0.02E_e)$. In Fig. 6 we show the bremsstrahlung cross section for two energies together with the compilation of Ref. [29].

Results of calculations of the dimuon yields $N^{\mu^+\mu^-}$ predicted by Eqs. (9) and (13) as a function of the primary electron energy E_e^0 are exhibited in Fig. 7. The total number of

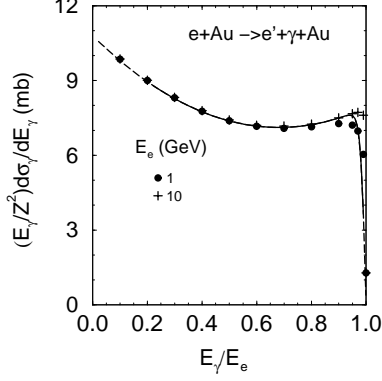


FIG. 6: The scaled bremsstrahlung cross section $(E_\gamma/Z^2)d\sigma_\gamma(E_e, E_\gamma)$ as a function of E_γ/E_e for two electron energies 1 GeV (solid curve) and 10 GeV (dashed curve). The symbols represent the data compilation of Ref. [29].

dimuons produced in eA interactions is about 1 and 60 for $E_e^0 = 1$ and 10 GeV, respectively for thick target. The yield increases with the thickness of the target. Some saturation sets in at $L \geq L_{\text{sat.}} \simeq 0.5$ cm. This means that the dimuons are essentially produced in a narrow region of the target mostly because of the large energy loss. It seems to be natural, because the saturation length $L_{\text{sat.}}$ is close to the scale parameter l_0 in Eq. (11).

The number of dimuons in γA interactions is about 200 and 6000 for $E_e^0 = 1$ and 10 GeV, respectively, for target thickness of 1 cm. The dependence of the total yield on the target thickness is rather strong due to the large mean free path of the bremsstrahlung photons.

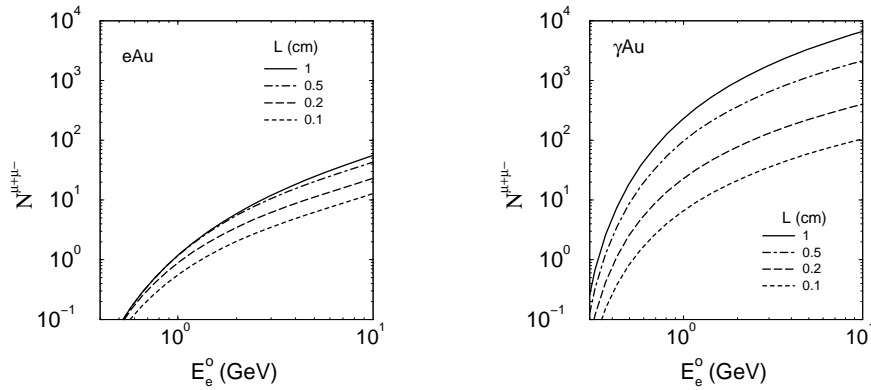


FIG. 7: The yields of dimuons in eA (left panel) and γA (right panel) interactions as a function of primary electron energy E_e^0 , calculated by Eqs. (9) and (13), respectively.

The dimuon yield in γA interactions considerably exceeds the corresponding yield in eA interactions. This excess strongly depends on the target thickness. Therefore, in Fig. 8

we present the total dimuon yield in interactions of relativistic electrons with a gold target which is a sum of the two above contributions as a function of the primary electron energy E_e^0 and target thickness L . For thick targets it practically coincides with the result shown

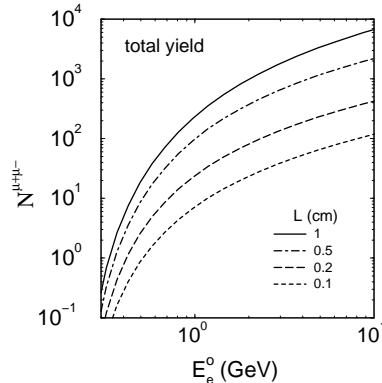


FIG. 8: The total yield of dimuons in interactions of relativistic electrons with the gold target as a function of the primary electron energy E_e^0 and target thickness L .

in Fig. 7 (right panel).

IV. BRIEF COMMENT ON HADRONIC PROCESSES

Finally, let us consider the hadronic sources of muons in interactions of the laser-wakefield accelerated electrons with the thick target. The main source of muons here is the photo and/or electro production and subsequent decay of π^\pm mesons in the elementary processes

$$\gamma + p \rightarrow \pi^+ + n, \quad \gamma + n \rightarrow \pi^- + p, \quad (16)$$

$$\gamma + N \rightarrow \pi^+ + \pi^- + N, \quad (17)$$

where γ stands for real bremsstrahlung photons (photoproduction) or virtual photons (electroproduction). The production of K mesons by 1 GeV electrons is strongly suppressed because of energy arguments, however, at higher energies they contribute to the muon production similarly to the pions. Charged pions decay via

$$\pi^+ \rightarrow \mu^+ + \nu_\mu, \quad \pi^- \rightarrow \mu^- + \bar{\nu}_\mu \quad (18)$$

with a probability of 99.99%. The cross sections of the reactions (16) and (17) for $E_\gamma \sim 1$ GeV are around $100 \mu\text{b}$ (see, for example, [30]). Pion photoproduction in γA reactions is

proportional to $A^{2/3}$. This means that the cross section of the muon production at heavy target nuclei by $\gamma A \rightarrow \pi^\pm X \rightarrow \mu^\pm + \nu_\mu(\bar{\nu}_\mu)X$ reactions exceeds the dimuon photoproduction, considered in previous section, by a factor of 20 – 30. Taking into account the large pion absorption cross section at heavy target nuclei by strong interaction processes this means that the produced pions will be essentially absorbed in a thick target. The target must be thin enough to get a well collimated muon beam. This condition reduces the muon yield considerably. For example, for a dozen μm thick gold target the expected yield of μ^\pm muons is less than 1 event for the above considered electron bunch. Therefore, the direct production of dimuons in electromagnetic interactions seems to be a more favorable mechanism.

V. SUMMARY

In summary we have considered muon pairs production by GeV electrons, created by a laser wakefield accelerator, impinging on a thick high- Z target. We estimated the effectiveness of a such a source of muon pairs. For a 1 cm thick gold target, 1.25×10^8 electrons in a 20 pC bunch with energy of 1 (10) GeV in the initial state produce about 2×10^2 (6×10^3) dimuons with pair energies centered at 1 GeV. To get 10^6 dimuons from the muon factory one needs $10^{10} - 10^{11}$ primary electrons in a bunch. Such intensities with power of 100 J seem to be quite realistic in near future, requiring ultra-high intensity laser pulses with efficient acceleration mechanisms. Cooling of the heat load in the target material analog to Ref. [31] may be an option for higher repetition rates. The produced muons, unlike electrons and hadrons, penetrate the target material without suffering noticeable scattering and absorption. Thus the configuration of a laser driven electron accelerator and thick high- Z target may serve as an all-optics table top device for muon pair production. The produced μ mesons may be used in studying various aspects of muon and neutrino physics and to be considered as an important step towards investigations of more complicated electron induced elementary processes.

Acknowledgments

The authors appreciate S.V. Bulanov, T.E. Cowan, and T.Zh. Esirkepov for fruitful discussions.

- [1] W.P. Leemans *et al.*, Nature Physics **2**, 696 (2006).
- [2] T. Tajima and J.M. Dawson, Phys. Rev. Lett. **43**, 267 (1979).
- [3] S. Karsch *et al.*, New J. Phys. **9**, 415 (2007).
- [4] J. Osterhoff *et al.*, Phys. Rev. Lett. **101**, 085002 (2008).
- [5] A. I. Titov and T. S. H. Lee, Phys. Rev. C **66**, 015204 (2002).
- [6] A. Donnachie and Yu.S. Kalashnikova, Phys. Rev. C **78**, 064603 (2008).
- [7] Y. S. Oh, A. I. Titov, and T. S. H. Lee, Phys. Rev. C **63**, 025201 (2001).
- [8] B. Saghai, J.-C. David, B. Julia-Diaz, and T.-S.H. Lee, Eur. Phys. J. **A 31**, 512 (2007).
- [9] S. Geer, Phys. Rev. D **57**, 6989 (1998) [Erratum-ibid. D **59**, 039903 (1999)].
- [10] S. Geer, J. Phys. G **29**, 1485 (2003).
- [11] A. Bandyopadhyay *et al.* [ISS Physics Working Group], arXiv:0710.4947 [hep-ph].
- [12] W. J. Marciano, T. Mori, and J. M. Roney, Ann. Rev. Nucl. Part. Sci. **58**, 315 (2008).
- [13] G. W. Bennett *et al.* [Muon g-2 Collaboration], Phys. Rev. D **73**, 072003 (2006).
- [14] S. V. Bulanov, T. Esirkepov, P. Migliozi, F. Pegoraro, T. Tajima, and F. Terranova, Nucl. Instrum. Meth. A **540**, 25 (2005).
- [15] K. Nakashima and H. Takabe, Phys. Plasmas **9**, 1505 (2002).
- [16] S. Karsch *et al.*, Laser Part. Beams, **17**, 565 (1999).
- [17] M. Ruf, G. R. Mocken, C. Muller, K. Z. Hatsagortsyan, and C. H. Keitel, Phys. Rev. Lett. **102**, 080402 (2009).
- [18] C. Muller, C. Deneke, and C. H. Keitel, Phys. Rev. Lett. **101**, 060402 (2008).
- [19] I. Kuznetsova, D. Habs, and J. Rafelski, Phys. Rev. D **78**, 014027 (2008).
- [20] A.I. Akhiezer and V.B. Berestetsky, Quantum Electrodynamics [Interscience, 1965].
- [21] G. Roche, C. Ducos, and J. Prortol, Phys. Rev. A **5**, 2403 (1972).
- [22] L. I. Schiff, Phys. Rev. **83**, 252 (1951).
- [23] E. Borie and H. Arenhoevel, Z. Phys. **255**, 459 (1972).

- [24] T. Tajima and G. Mourou, Phys. Rev. ST Accel. Beams **12**, 051302 (2002).
- [25] G. A. Mourou, T. Tajima, and S. V. Bulanov, Rev. Mod. Phys. **78**, 309 (2006).
- [26] N. Kirby *et al.*, Phys. Rev. ST Accel. Beams **12**, 051302 (2009).
- [27] P.L. Schkolnikov, A.E. Kaplan, A. Pukhov, and J. Meyer-ter-Vehn, Appl. Phys. Lett. **71**, 3471 (1997).
- [28] A.P. Babichev *et al.*, Physical Values. Hand-book, (Eds). I.S. Grigoriev and E.Z. Meilikhov. Energiatomizdat, 1991 (in Russian).
- [29] S.M. Seltzer and M.J. Berger, At. Data Nucl. Data Tables, **35**, 345 (1986).
- [30] S. Schadmand, Pramana **66**, 877 (2006) [arXiv:nucl-ex/0505023].
- [31] J. Klug *et al.*, Nucl. Instrum. Meth. A **577**, 641 (2007).